Petroleum Science 20 (2023) 2372–2385

Contents lists available at ScienceDirect

Petroleum Science

journal homepage: www.keaipublishing.com/en/journals/petroleum-science

Original Paper

Modeling the hydration, viscosity and ultrasonic property evolution of class G cement up to 90 °C and 200 MPa by a scale factor method

Li-Jun Sun [a], Xue-Yu Pang [a, b, *], Siavash Ghabezloo [c], Hai-Bing Yan [d]

[a] School of Petroleum Engineering, China University of Petroleum (East China), Qingdao, 266580, Shandong, PR China
[b] Key Laboratory of Unconventional Oil & Gas Development (China University of Petroleum (East China)), Ministry of Education, Qingdao, 266580, Shandong, PR China
[c] Navier, Ecole des Ponts, Univ Gustave Eiffel, CNRS, Marne-la-Vallee, France
[d] CNPC Chuanqing Drilling Engineering Co. Ltd. (CCDC), Chengdu, 610051, Sichuan, PR China

ARTICLE INFO

Article history:
Received 11 May 2022
Received in revised form
17 January 2023
Accepted 17 January 2023
Available online 20 January 2023

Edited by Yan-Hua Sun

Keywords:
Activation energy
Activation volume
Isothermal calorimetry
Consistency
Ultrasonic property

ABSTRACT

A comprehensive experimental program has been performed to characterize the hydration and engineering property evolution of a class G oil well cement under various curing temperatures from 30 to 90 °C. The progress of hydration was monitored by isothermal calorimetry (atmospheric pressure); the viscosity evolution was measured using a high temperature and high pressure consistometer (up to 200 MPa); the ultrasonic property development was evaluated by an ultrasonic cement analyzer (up to 100 MPa). Test results indicate that the influences of curing temperature and pressure on the hydration, viscosity and ultrasonic property development can be modeled by a scale factor method that is similar to the maturity method used in the concrete industry. However, the key parameters of the scale factor model, namely the apparent activation energy and the apparent activation volume of cement showed obvious variations with test method and curing condition. The test results indicate that the curing temperature has a stronger effect on cement hydration rate than viscosity and ultrasonic property development rate, while the curing pressure has a much stronger influence on cement slurry properties before setting (viscosity) than after setting (ultrasonic property).

1. Introduction

A series of physical and chemical reactions of cement slurry will take place when dry cement is mixed with water; various properties of cement-based materials will continue to evolve with the extension of hydration time, such as viscosity (Scherer et al., 2010) and rheology (Ma and Kawashima, 2019) of a cement slurry, as well as compressive strength (Du et al., 2018; Kjellsen et al., 1991), permeability, and elastic modulus (Krauβ and Hariri, 2001) of a set cement. For well cementing, due to the effect of the geothermal and geopressure gradient (about 27 °C/km for temperature) (Ma and Kawashima, 2019), temperature and pressure of oil well cement placed downhole will increase with the increase in wellbore depth (API RP 10B-2, 2013). In other words, oil well cement will undergo wide ranges of temperature and pressure changes in a wellbore. For a given cement slurry, curing temperature and curing pressure are two of the most important factors affecting the hydration process (Pang et al., 2013a, 2013b, 2013c) and the resulting microstructure (Gallucci et al., 2013). Both curing temperature and curing pressure can accelerate the hydration rate of cement during the early stage of cement hydration. In addition, temperatures above 110 °C will change the hydration products of cement to crystalline phases, which will directly lead to significant changes in the long-term performance of cement-based materials (Taylor, 1997). Therefore, to optimize cement slurry formulation and improve cementing quality, it is of considerable practical significance to study and accurately predict the property evolution of cement-based materials with time under the influence of different temperatures and pressures.

All wellbore integrity analysis software requires mechanical properties of oil well cement as critical input parameters (Meng et al., 2021). Understanding and simulating the engineering property evolution of oil well cement is essential for the design

* Corresponding author. School of Petroleum Engineering, China University of Petroleum (East China), Qingdao, 266580, Shandong, PR China.
E-mail address: x.pang@upc.edu.cn (X.-Y. Pang).

https://doi.org/10.1016/j.petsci.2023.01.014

optimization of oil well cement system and long-term integrity of cement sheath. Previous publications have shown that hydration kinetics studies of Portland cement can be very useful in the simulation of cement property evolutions (Sun et al., 2021a, 2021b). The experimental methods used to obtain cement hydration kinetics data include quantitative X-ray diffraction analysis (QXRD) (Pang et al., 2022; Kupwade-Patil et al., 2019; Jupe et al., 2012a, 2012b; Bergold et al., 2013; Jansen and Goetz-Neunhoeffer, 2012; Hesse et al., 2011), bound water content analysis (Pang et al., 2022; Escalante-Garcia, 2003; Gómez-Zamorano and Escalante-García, 2010; Li et al., 2014; Chidiac and Shafikhani, 2019; Liao et al., 2019), isothermal calorimetry (IC) (Pang et al., 2013a, 2013b, 2021; Sun et al., 2021b), and chemical shrinkage (Pang et al., 2013a, 2013c; Lura et al., 2010; Peethamparan et al., 2010; Pang and Meyer, 2012). Among them, the IC method is most widely used since it can directly and continuously collect high-precision heat flow data of the hydration process. For oil well cement, viscosity and compressive strength are two of the most important time-evolving engineering parameters. The rate of increase in viscosity of cement slurry should not be too slow or too fast for the safety and efficiency of cementing operation. After the cement slurry is pumped into place, the cement sheath must achieve a sufficiently high compressive strength before next section can be drilled. Unlike traditional methods of measuring cement viscosity and compressive strength, which are generally carried out at sparsely spaced discrete time points, the petroleum industry provides means of indirect continuous measurement of the two parameters through high-temperature and high-pressure (HTHP) consistometers and ultrasonic cement analyzers (UCA), respectively. The objective of this study is to carry out a comprehensive study of oil well cement hydration kinetics, investigate its correlations with engineering properties, and develop relevant models to simulate the property development and to deepen our understanding of cement hydration process.

A maturity model that was developed mainly based on Arrhenius' law was initially used to predict the development of compressive strength of set cement in the early stage (Zhang et al., 2008). The model was later extended to predict other property development of cement-based materials (Zhang et al., 2008; Delatte et al., 2000; Kada-Be et al., 2000; Kjellsen and Detwiler, 1992; Jensen and Hansen, 1999; Pinto and Hover, 1999; Turcry et al., 2002). Pang et al. (Pang et al., 2013b, 2013c) has developed a scale factor model to simulate the influence of temperature on hydration kinetics and property development of oil well cement based on similar principle as the maturity model. In these models, the apparent activation energy (E_a) can provide information about the sensitivity of cement hydration reaction to temperature for a constant pressure process. The apparent activation volume (ΔV^*) can be used to characterize the sensitivity of cement hydration processes to curing pressure for a constant temperature process. Using the scale factor model, Pang et al. (Pang, 2014; Pang et al., 2014) also conducted preliminary explorations on the simulation of certain engineering performance of oil well cement; however, previous validations of the model are mostly limited to the temperature range of 15–60 °C and the pressure range of 5–50 MPa, which is too small considering the actual application environment of oil well cement.

During this study, a comprehensive investigation of hydration kinetics and property evolution of a Class G oil well cement in the temperature range of 30–90 °C was conducted. Various experimental methods (IC, HTHP consistometer, UCA) were employed during this study. Due to equipment limitations, IC tests were conducted at atmospheric pressure, while HTHP consistency and UCA tests were conducted at maximum pressures of 200 and 100 MPa, respectively. The scale factor model was used to study and predict the effect of temperature and pressure on property evolution of oil well cement with time. The dependence of E_a and ΔV^* on curing temperature and pressure was analyzed. Finally, the difference of E_a obtained by different experimental methods as well as ΔV^* was studied.

2. Theoretical background

Previous studies (Pang et al., 2013a, 2013b, 2013c, 2021) have found an interesting phenomenon that cement hydration kinetics curves under the influences of different curing conditions (temperature and pressure) as well as several chemical additives have similar shapes, when they were represented by the rate of hydration as a function of the degree of cement hydration. These studies suggest that there are proportional relationships between the hydration rates under different conditions for the same degree of hydration. Therefore, the hydration kinetic curve under arbitrary curing conditions can be predicted based on that of a reference condition by a scale factor (C) model. The scale factor describes the difference in cement hydration rate caused by the change of curing conditions compared to the reference condition, which reflects the dependence of cement hydration rate on curing conditions. It can be written as (Pang et al., 2013b, 2013c):

$$C_{(T_r \to T, P_r \to P)} = \exp\left(\frac{E_a}{R}\left(\frac{1}{T_r} - \frac{1}{T}\right) + \frac{\Delta V^*}{R}\left(\frac{P_r}{T} - \frac{P}{T}\right)\right) \tag{1}$$

where E_a is the apparent activation energy, kJ/mol; R is the gas constant (8.314 J/(mol K)); ΔV^* is the apparent activation volume, m^3/mol; T is the arbitrary temperature, K; P is the arbitrary pressure, MPa; T_r and P_r are the reference temperature (K) and the reference pressure (MPa), respectively.

In the scale factor model, if it is assumed that the cement hydration kinetics under the reference curing condition (T_r, P_r) can be expressed by the following mathematical function:

$$\alpha = f(t) \tag{2}$$

Then, the cement hydration under the effect of any arbitrary curing conditions (T, P) can be expressed by the following equation (Pang et al., 2013b, 2013c):

$$\alpha = f(C(t - t_0)) \tag{3}$$

where f is the function representing the time dependence of the degree of hydration (α) at temperature T; t_0 is an offset time, h, which was introduced to account for the potentially different hydration mechanism during the very early period (before the end of the induction period), which may have a different temperature and pressure dependence than the main hydration. This is to say that the end of induction period may not be predicted correctly using a scale factor derived from the main hydration stage.

As mentioned earlier, cumulative heat of hydration can be used to study cement hydration kinetics because it has a linear relationship with the degree of cement hydration. Similarly, the scale factor model can also be applied to other properties (i.e. rheology/viscosity, ultrasonic strength, and ultrasonic transit time) that have an approximately one to one relationship with the degree of cement hydration. We can simulate the evolution of these cement properties under the influence of curing temperature and pressure based on the scale factor model as well. If it is assumed that a certain property (x) evolution of a cement slurry under the reference temperature and pressure (T_r, P_r) can be expressed by Eq. (4).

$$x = x_{T_r,\, P_r}(t) \tag{4}$$

Then, the property evolution of cement slurry at arbitrary temperature and pressure conditions (T, P) can be expressed by Eq. (5).

$$x = x_{T\,,\,P}(t) = x_{T_r\,,\,P_r}(C(t - t_0)) \tag{5}$$

Because the above mathematical formulas are derived for isothermal and isobaric data, a numerical approach is needed to convert test data at variable temperature and pressures using the equivalent age concept. When temperature and pressure vary with time, the equivalent age t_e at the reference curing condition (T_r, P_r) corresponding with the actual curing age t at any arbitrary temperature and pressure condition ($T(t)$, $P(t)$) can be described by the following formula (Pang et al., 2014, 2020, 2021):

$$t_e = \sum_{i=1}^{n} \exp\left(\frac{E_a}{R}\left(\frac{1}{T_r} - \frac{1}{T(t_i)}\right) + \left(\frac{\Delta V^*}{R}\left(\frac{P_r}{T(t_i)} - \frac{P(t_i)}{T(t_i)}\right)\right)\right)\Delta t_i \tag{6}$$

where Δt_i is the infinitesimal time increment at t_i; $T(t_i)$ is the average temperature between time t_i and time t_{i+1}; $P(t_i)$ is the average pressure between time t_i and time t_{i+1}. Because the time interval is very small, $T(t_i)$ and $P(t_i)$ can also be taken as the temperature and pressure at time t_i. The experimental data of a certain property development as a function of the equivalent age can be fitted with an empirical equation and the test results at any arbitrary temperature and pressure history can then be predicted using that equation. This is similar to the maturity method used to estimate compressive strength of concrete materials in the civil engineering industry (ASTM C1074-19, 2019). In addition to using an empirical fitting, one can also use the interpolation method to make the prediction based on the property vs. equivalent age curve numerically. More details on how to use the numerical approach can be found in Pang et al. (Pang et al., 2014, 2020).

3. Experimental materials and methods

3.1. Experimental materials and slurry preparation

Class G oil well cement with a density of 3.25 g/cm^3 and a median particle size of 19.5 μm were obtained from Aksu cement factory, Xinjiang, China. The cement used in this study was from the same production batch supplied by the same manufacturer as the cement used in our recent study. More detailed information about the cement such as particle size distribution, compound compositions and X-ray diffraction profile can be found in Pang et al. (2021).

During this study, all slurries were prepared by mixing 224 g of tap water with 560 g of cement in a laboratory cement slurry blender at room temperature according to standard API procedures (API RP 10B-2, 2013), which is close to a neat slurry with a water-to-cement ratio (W/C ratio) of 0.4. Small amounts of several chemical additives were added to the slurry to obtain desirable slurry properties, such as good mixability, and sedimentation stability, which includes a suspension aid (diutan gum, 0.05% by weight of cement, or BWOC), a dispersant (20% activity, BCD-210L, 1.25% BWOC), and a defoamer (G603, 0.3% BWOC).

3.2. Isothermal calorimetry test

Isothermal calorimetry (IC) tests were performed using a Calmetrix isothermal calorimeter (model: I-Cal Ultra, USA) to measure the heat flow rate during cement hydration at the curing temperature range of 30–90 °C under atmospheric pressure, following ASTM C standard test procedure (ASTM C1608, 2017). A sample of approximately 12.0 g was transferred to a plastic vial and sealed with a cap immediately after the cement slurry was mixed. Generally, it takes approximately 5 min to place the sample into the calorimeter after mixing. Timing of each test starts at the point when the sample was placed inside the calorimeter. Testing data during the first hour were discarded because approximately 1 h is required for the test to reach an equilibrium state to collect accurate heat-flow data.

3.3. Thickening time test

An HTHP consistometer (purchased from China Liaoning Bassrett Petroleum Equipment Manufacturing Co., LTD., model: BSRD-8042DG) was used to measure the viscosity evolution of a cement slurry at various conditions, within the temperature range from 30 to 90 °C and pressure range from 5 to 200 MPa. The viscosity of cement slurry is determined from the torque exerted on a set of stationary paddles immersed in the slurry while the slurry cup is rotating at 150 rpm. It is expressed in Bearden consistency (Bc) units and has a linear relationship with torque. Generally, when the consistency of cement slurry reached 70 Bc, it is considered to have reached the limit of pumpability (LOP). The time required to reach LOP is called the thickening time. In this study, it takes about 50 min to ramp up the temperature and pressure from ambient condition to the target curing condition.

3.4. Ultrasonic cement analyzer test

The measurement of cement compressive strength is traditionally performed by destructive crush testing using a load frame. Nondestructive testing by ultrasonic methods based on either wave reflection method or wave transmission method is also widely used to monitor the setting and hardening process of cementitious materials (Voigt et al., 2006; Reinhardt and Grosse, 2004; Lee et al., 2004; Robeyst et al., 2008; Zhang et al., 2012). In general, good correlations were found between ultrasonic properties and compressive strength. In this study, an ultrasonic cement analyzer (UCA) by Chandler Engineering was used to measure the ultrasonic property (transit time of compressional wave through the sample) evolution of oil well cement at various conditions, within the temperature range from 30 to 90 °C and pressure range from 5 to 100 MPa. The ultrasonic transit time is converted to sonic compressive strength based on a proprietary empirical equation in the data acquisition software. It takes about 50 min to ramp up the temperature and pressure from ambient condition to the target curing condition during these tests.

4. Test results and discussion

4.1. IC test results

In the range of 15–95 °C, the effect of curing temperature on the hydration heat evolution of Portland cement is well understood from our previous study (Pang et al., 2021). Fig. 1 shows the hydration kinetic mechanism curves of Aksu Class G cement at various temperatures as measured by isothermal calorimetry. The shapes of hydration kinetics curves are very similar in the temperature range from 15 to 79 °C. However, the shapes of hydration curves at higher temperatures (87 °C and above) started to show significant variations with temperature. Dual peaks appeared under high curing temperature, which is likely caused by accelerated reaction of the aluminate phases. Therefore, in the lower temperature range (30–79 °C), the scale factors can be conveniently derived by calculating the ratios of hydration peaks between different tests (i.e. the main peak value of the hydration rate curve under any condition is divided by that under a reference condition),

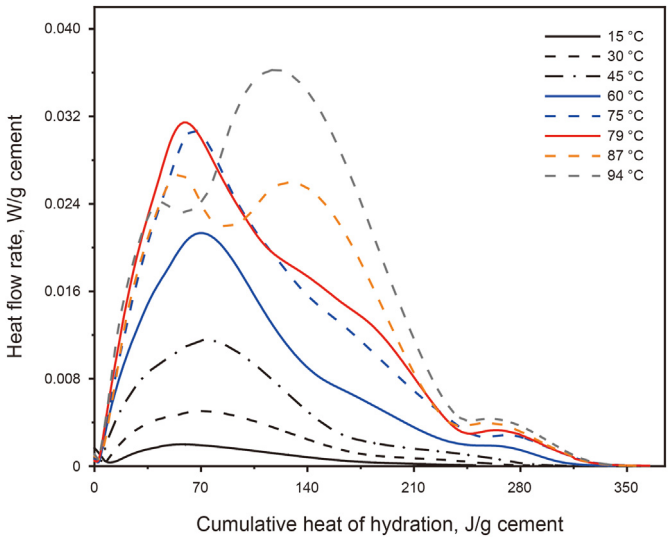

Fig. 1. Heat flow vs. cumulative heat of hydration of Aksu Class G cement.

which is known as the peak ratio method; in the higher temperature range, the scale factors have to be obtained by the best fit method (where hydration kinetics at one condition is transformed to achieve the best fit with that at another condition) (Pang et al., 2013a).

The model parameters obtained by both methods at different curing temperatures are shown in Table 1. For the test results between 30 and 60 °C, the scale factor obtained by both methods agreed very well. The values of E_a calculated based on Eq. (1) for different temperature ranges were in good agreement with previous studies. Compared to lower temperature tests (30–60 °C), the values of E_a decreased significantly in the higher temperature range (60–94 °C). A more appropriate method of deriving E_a to account for a wider temperature range is by linear regression analysis (Fig. 2). It can be seen from Table 1 and Fig. 2 that E_a derived in the temperature range of 30–60 °C by linear regression analysis was more than 40 kJ/mol, but became significantly lower (18.3 kJ/mol) in the temperature range of 60–94 °C.

In this article, variable references and the scale factor estimated by the best fit method were used to simulate the cement hydration curve under different curing temperatures (Fig. 3). Nearest temperature data curves were used as references for the predictions (e.g. 30 °C results used to predict 45 °C results and 45 °C results used to predict 60 °C results, etc.). The same quality of fit can also be obtained by using the middle temperatures (e.g. using 30 °C results to predict both 15 °C and 45 °C results). As discussed in previous studies, the prediction results were more accurate when using the nearest temperature data curve as the reference curve (Sun et al., 2021b). This is because smaller temperature differences led to smaller changes in hydration mechanism. The reasonable agreements in the results suggested that the scale factor model was still valid in the temperature range from 60 to 94 °C. The errors in the cumulative heat evolution between experimental data and predicted data for all temperature tests at 50 h are within 6.0%. It should be pointed out that time offsets as shown in Eq. (3) were used in the model results here to account for the different mechanism of cement hydration during the early hydration (before the main reaction).

4.2. Thickening time test results

The effect of curing temperature on the consistency evolution profiles of Aksu cement slurry at 5 and 50 MPa are shown in Fig. 4, which exhibited very similar trends. In general, with increasing curing temperature, the rate of consistency evolution increases, except for the temperature range from 75 to 90 °C. It is clear that the thickening time of cement slurry decreased with increasing temperature up to 75 °C at both curing pressures. High temperature significantly decreased thickening time of cement slurry, which is mainly because the elevated temperature can promote rapid nucleation and growth of cement hydration products (Scherer et al., 2010). The measured thickening time of cement slurry was reduced from 3.94 h at 30 °C to 1.86 h at 75 °C at 50 MPa; while it was reduced from 8.37 h at 30 °C to 2.52 h at 75 °C at 5 MPa. The thickening time at 75 °C was slightly shorter than that at 90 °C for both curing pressures. This phenomenon is known as thickening time inversion and can adversely influence wellbore integrity during well cementing (cement at shallower depth may set faster than that at higher depth). There are many possible explanations to the thickening time inversion phenomenon. For example, it may be attributed to cement hydration product change (ettringite decomposition) in this temperature range (Sun et al., 2022). Ettringite is known to have a needle-shaped structure (Taylor, 1997) and can cause more significant viscosifying effect than other hydration products. At the same time, increasing temperature can cause thermal thinning of cementing fluids, resulting in a lower slurry viscosity at the same degree of cement hydration. Considering that the temperature acceleration effect is much weaker in the range between 75 and 90 °C, it is also possible that thermal thinning effect overpowers acceleration effect on cement hydration in this range.

Based on the scale factor model presented in this study, the consistency evolution curves of cement slurry at different curing conditions should overlap when plotted as a function of the equivalent age using a fixed temperature and pressure as the reference curing condition according to Eq. (6). These curves can also be further transformed to predict the consistency evolution at any arbitrary conditions (Pang et al., 2014). However, the key parameters (E_a and ΔV^*) have to be changed to obtain the best agreements because of their dependence on temperature and pressure; this method is similar to the best fit method in hydration kinetics modelling mentioned previously in Section 4.1. Fig. 5 shows the prediction of HTHP consistency evolution profiles of

Table 1
Scale factor model parameters obtained from IC tests by two different methods at different temperature ranges.

T_r–T, °C	Best fit method				Peak ratio method			
	C	t_0, h	E_a, kJ/mol	E_a*, kJ/mol	C	t_0, h	E_a, kJ/mol	E_a*, kJ/mol
30–45	2.25	2.35	43.35	44.01	2.29	2.2	44.29	40.47
45–60	2.15	1.8	44.97		1.85	1.3	36.14	
60–74	1.55	1.5	30.10	18.30	1.44	1.3	25.04	–
74–87	1.12	0	9.25		N/A	N/A	N/A	N/A
87–94	1.08	0	12.09		N/A	N/A	N/A	N/A

Note: E_a* is the value of E_a derived in wider temperature ranges by linear regression analysis.

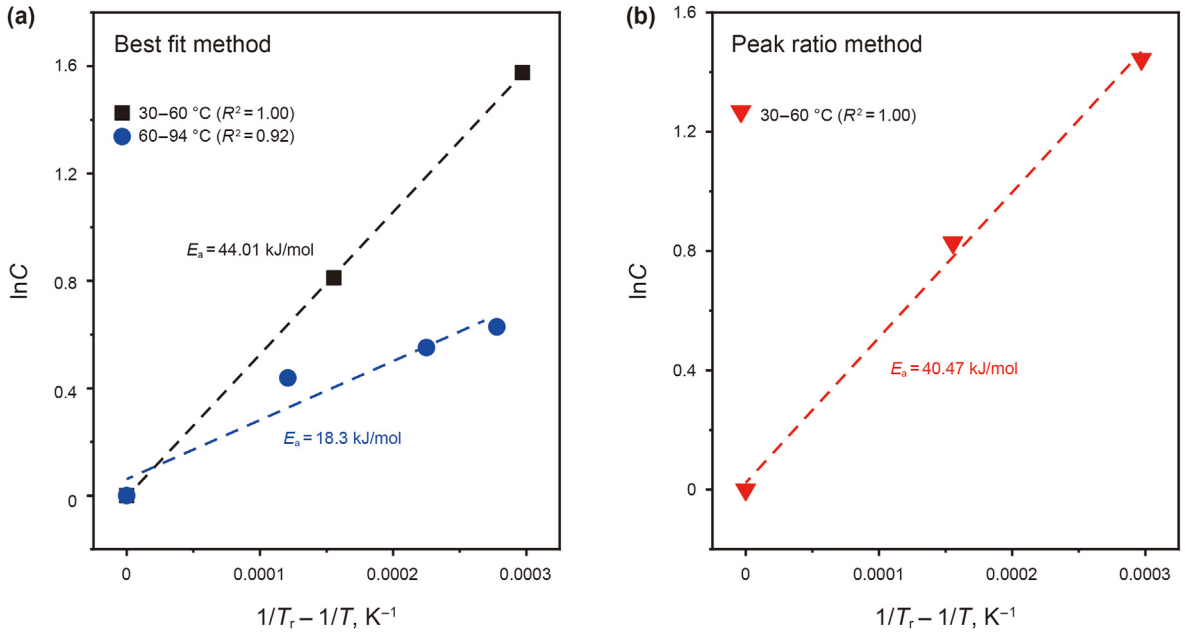

Fig. 2. Linear fits used to obtain the activation energy for Aksu Class G cement based on Eq. (1).

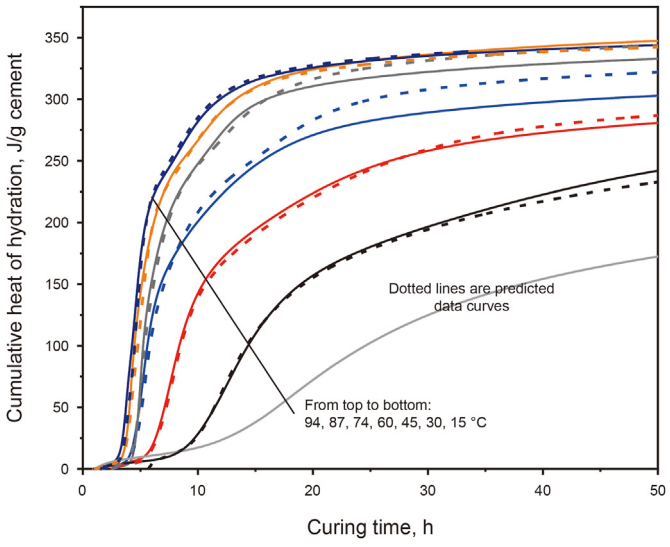

Fig. 3. Prediction of hydration kinetics at different temperatures by the scale factor model for Aksu Class G cement (using nearest temperature curves as references).

cement slurry at different temperatures at 5 and 50 MPa based on the best fit method using a ΔV^* of −24 cm^3/mol (Pang et al., 2013b) and an E_a that varies with the target temperature (The actual values used for different temperature ranges are listed in Table 2). As discussed previously in Section 2, before the prediction, the experimental data were first transformed into equivalent age data at isothermal and isobaric condition using a reference condition by Eq. (6) and fitted with an empirical equation (a sixth order polynomial in this case). It can be seen from Fig. 5 that the predicted curves of each test were in good agreement with the experimental data curves for both curing pressures. Similar to IC, the prediction was made by using the nearest temperature data curve as the reference. It can also be observed that consistency evolution profile of a cement slurry under different curing conditions was not always smooth and often showed a pattern of stepped increase; such details may be related to the unsynchronized reactions of different phases in cement or the generation and transformation of certain unstable hydrate phases, which is nearly impossible to predict. This phenomenon is less obvious at high temperatures because of the overall fast reaction rate of cement, so the predicted experimental results at high temperatures are in better agreements than at low temperatures.

Cement hydration reaction is the sum of a series of simultaneous chemical reactions rather than a single reaction process. According to Eq. (1), E_a represents the temperature sensitivity of the overall cement hydration reaction for a constant pressure process and is often called the apparent activation energy. As shown in Table 2, for both curing pressures, E_a derived from thickening time test data obtained here suggested that it decreased with increasing curing temperature, which is consistent with the IC test results of this study (Section 4.1) as well as previous studies (Pang et al., 2013a, 2021). However, the values of E_a seemed to be lower than those obtained from IC tests. For the same temperature range, the calculated E_a at 50 MPa was lower than that obtained at 5 MPa. With pressure increasing from 5 to 50 MPa, the magnitude of reduction of E_a in the lower temperature range (30–60 °C) was approximately 26%–35%, significantly larger than the 7% reduction in the higher temperature range (60–75 °C).

Fig. 6 illustrates the effect of different curing pressures on the consistency evolution of cement slurry at 30 and 75 °C. The experimental results showed that with increasing curing pressure, the development of cement slurry consistency was accelerated. The measured thickening time under 75 °C was reduced from 2.51 h at 5 MPa to 0.85 h at 200 MPa, while the thickening time under 30 °C was reduced from 8 h at 5 MPa to 1.1 h at 200 MPa. Such phenomenon of the effect of pressure on the consistency evolution was similar to that of temperature. In a previous study, it was also proved that curing pressure can accelerate cement hydration by isothermal calorimetry (Pang et al., 2013b). As shown in Fig. 6, the scale factor model was suitable for predicting the consistency evolution curve under different pressures. To account for the temperature variations during the ramp period, a constant E_a of 21.35 kJ/mol was used (derived based on the average results by

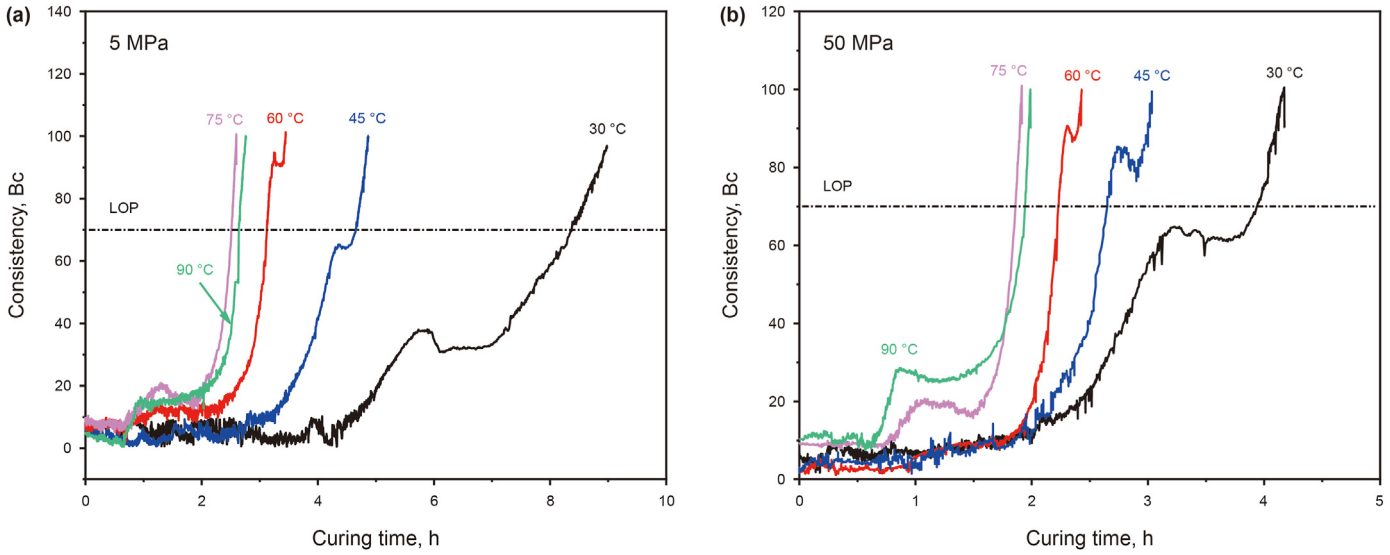

Fig. 4. Viscosity evolution of cement cured at different curing temperatures.

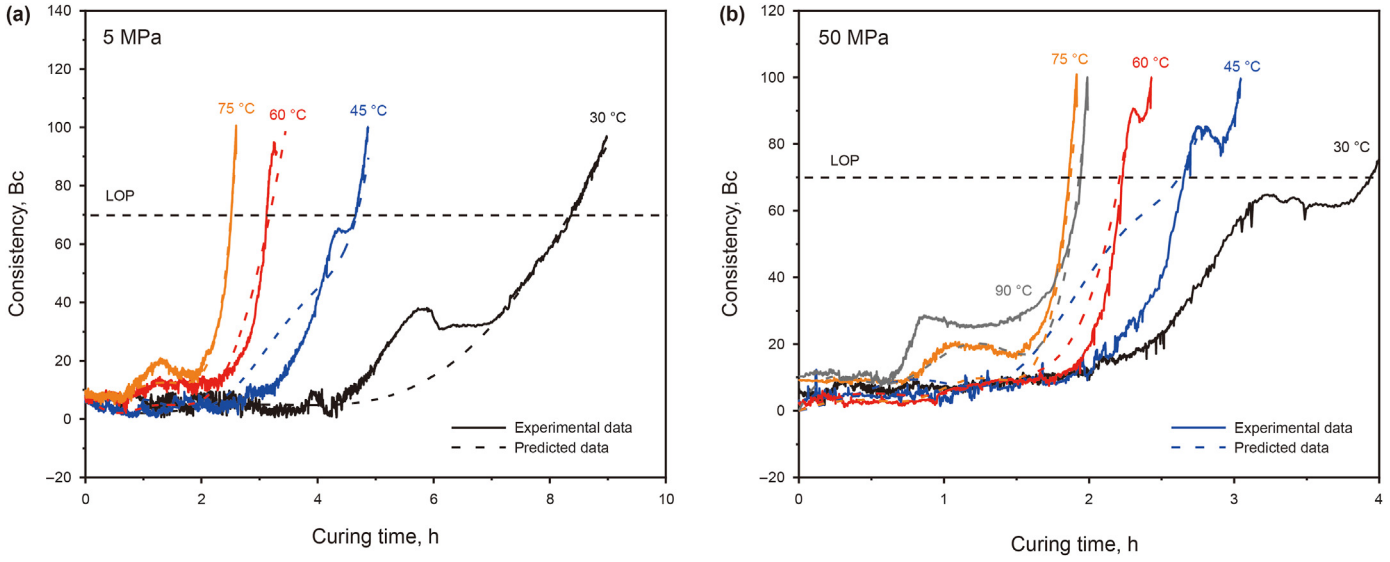

Fig. 5. Experimental and predicted consistency evolution of cement cured at different temperatures (nearest temperature data curve as reference).

Table 2
Scale factor model parameters obtained from thickening time tests at different temperature and pressure conditions.

T_r–T, °C	Parameters obtained at 5 MPa			Parameters obtained at 50 MPa		
	C	E_a, kJ/mol	E_a*, kJ/mol	C	E_a, kJ/mol	E_a*, kJ/mol
30–45	1.89	34	24.6	1.60	25	18.1
45–60	1.48	23		1.29	15	
60–74	1.26	15		1.24	14	
74–87	0.95	N/A	N/A	0.97	N/A	N/A

Note: E_a* is the value of E_a derived in wider temperature ranges by linear regression analysis.

linear regression presented in Table 2), while ΔV^* varies with the target pressure (The actual values for different pressure ranges are listed in Table 3). For tests at both temperatures, the predicted profiles of viscosity evolution of cement slurry at different pressures show excellent agreements with experimental curves. Compared with the results at different temperatures (Fig. 5), the prediction results at different pressures were more accurate, especially for high-temperature tests.

ΔV^* of cement in the scale factor model represents the pressure sensitivity of the overall cement hydration reaction for a constant temperature process. As shown in Table 3, with the change of pressure, ΔV^* derived by thickening time test data does not show an obvious trend of change with temperature and pressure. The variations in test results could be attributed to experimental uncertainties, as only one test was performed per curing temperature and pressure. The calculated values of ΔV^* at 30 °C were very high at pressures below 100 MPa and then became extremely small in the pressure range between 100 and 200 MPa. Except for the test results at 30 °C, most of the calculated values of ΔV^* are in good agreement with previous studies (Scherer et al., 2010; Pang et al., 2013b, 2014), with an average of −29.8 cm^3/mol and a standard deviation of 4.3 cm^3/mol.

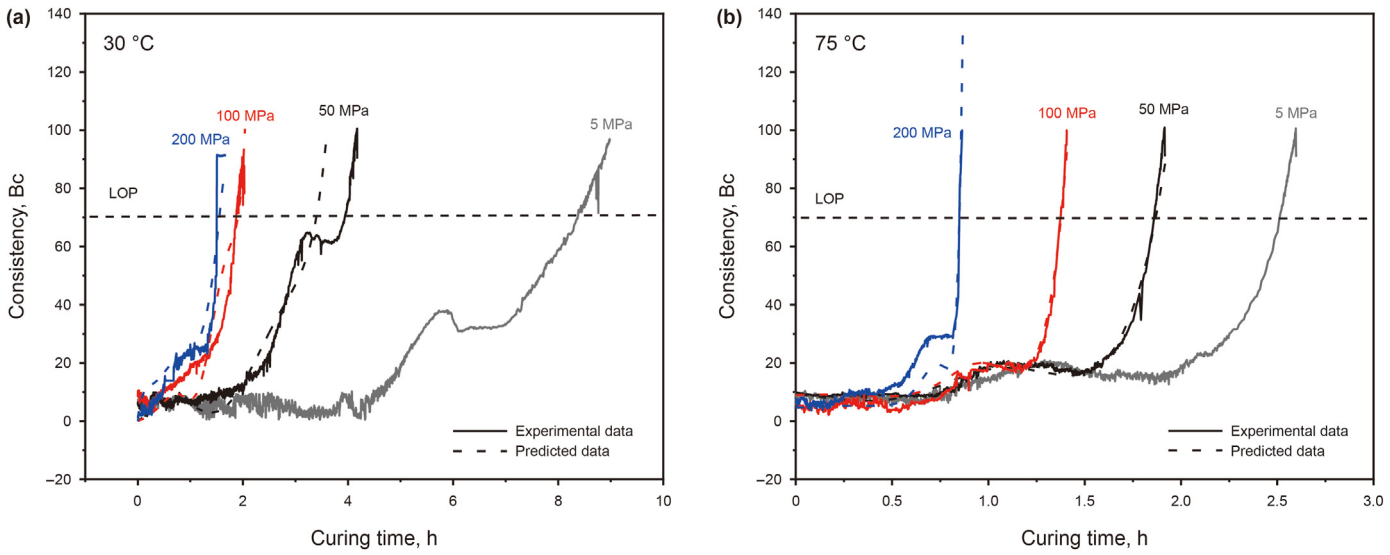

Fig. 6. Experimental and predicted consistency evolution of cement cured at different pressures (nearest pressure data curve as reference).

Table 3
Apparent activation volume (ΔV^*) obtained from thickening time tests at different temperature and pressure conditions (cm^3/mol).

Pressure, MPa	Apparent activation volume (ΔV^*) at different temperatures, cm^3/mol				
	30 °C	45 °C	60 °C	75 °C	90 °C
5–50	−55.5	−33	−28	−25.3	−28.3
50–100	−46.0	–	–	−27.3	–
100–200	−4.0	–	–	−37.0	–

4.3. UCA test results

As mentioned previously, the raw data obtained from UCA test was the transit time, but the purpose of conducting UCA tests was mainly to probe the mechanical property evolution of the cement in a nondestructive way. Therefore, transit time was converted to ultrasonic compressive strength (CS) and compressional wave (P-wave) velocity and their evolution with time at various curing conditions are shown in Fig. 7. Theoretically, the P-wave velocity is proportional to the square root of the dynamic odometer modulus of the cement. As the curing temperature is increased, the evolution rate of ultrasonic CS as well as P-wave velocity of the setting cement are significantly accelerated in the lower temperature range of 30–45 °C during early hydration periods. The time it took for ultrasonic property to reach a stable stage generally decreased with increasing temperature. Both test results were qualitatively similar to IC (Section 4.1) and thickening time test (Section 4.2) in that the influence of temperature seemed to be significant in the lower temperature range (30–45 °C) but became smaller at higher curing pressures and higher temperatures. For the test results at 5 MPa, the rate of the ultrasonic CS and P-wave velocity evolution at 75 °C was significantly faster than that of 90 °C. This behavior agrees with crush strength of the cement tested previously (Pang et al., 2022) and was similar to the reversed trend of thickening time test results from 75 to 90 °C in Fig. 4. For the test results at both 50 and 100 MPa, the ultrasonic CS and P-wave velocity evolution curves almost overlapped in the temperature range from 60 to 90 °C, suggesting very minimal influences from curing temperature at high curing pressure conditions. Ultrasonic CS derived at lower temperatures (30 °C and sometimes 45 °C) were significantly higher than those derived at higher temperatures at the late hydration period (see in Fig. 7a–c). It may be because the microstructure of cement samples cured under lower temperatures is finer and more homogenous than that under higher temperatures (Gallucci et al., 2013).

A simple empirical function as described by Eq. (7) is widely used to simulate both hydration kinetics and strength evolution of cement-based materials (ASTM C1074-19, 2019; Chidiac et al., 2013; Pichler et al., 2017). Clearly the function can be considered as a specific example of Eq. (5) to simulate ultrasonic strength development. The rate constants (k) in this model can be used to calculate the scale factor and derive the activation energy and activation volume parameters (Pang et al., 2022).

$$S = S_u \frac{k(t - t_0)}{1 + k(t - t_0)} \tag{7}$$

$$C = \frac{k_{T,P}}{k_{T_r,P_r}} \tag{8}$$

where S is the ultrasonic compressive strength of cement at time (curing age) t; S_u is the ultimate/limiting strength; t_0 is the time when strength development is assumed to begin; k is the rate constant for the ultrasonic compressive strength development (the subscripts are the corresponding temperature and pressure under consideration).

Since the ultrasonic CS is derived from transit time using an empirical equation and P-wave velocity is calculated by taking the inversion of transit time, it is probably more appropriate to directly analyze the raw transit time test data using a similar model as Eq. (7). Because a cement slurry is in liquid stage in the initial stage of hydration, it takes longer for the ultrasonic wave to pass through the sample and the entire hydration process is accompanied by transit time reduction. A slight modification to the equation is need to simulate the sonic transit time development curve as the initial value is nonzero. The following equation was proposed (Pang et al., 2022):

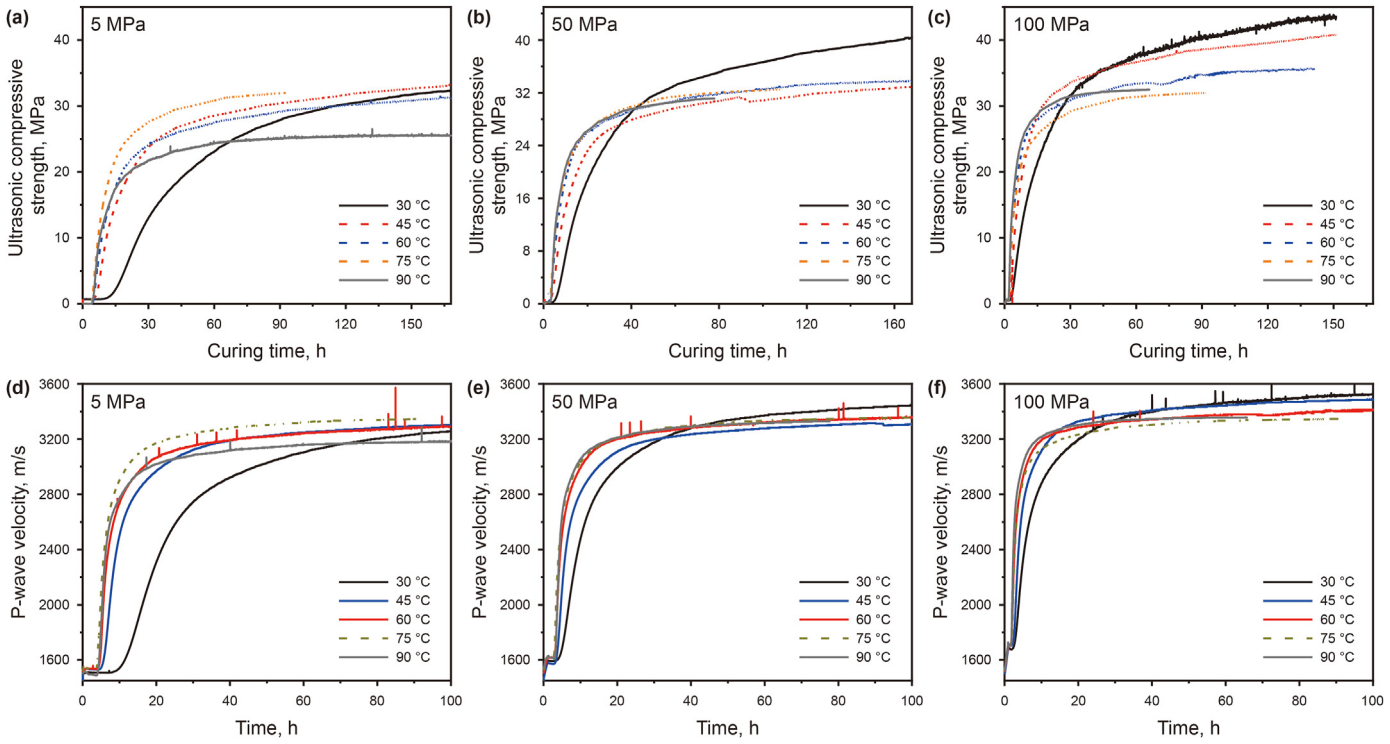

Fig. 7. Effect of temperature and pressure on the evolution of ultrasonic CS as well as P-wave velocity through the setting cement by UCA.

$$t_S = t_S^I + t_S^u \frac{k_S^t (t - t_0)}{1 + k_S^t (t - t_0)} \tag{9}$$

where t_S^I and t_S are the sonic transit time at time 0 and time t, respectively; t_S^u is the ultimate change in transit time, which is a negative value; k_S^t is the rate constant. In the generalized scale factor model, it is basically assumed that the rate constants of ultrasonic property evolution (i.e. k in Eq. (7) and k_S^t in Eq. (9)) have similar relationships with curing temperature and pressure as hydration reaction rate constants. In addition to the scale factor model (represented by Eqs. (1) and (8)), the rate constants in Eqs. (7) and (9) may also be directly employed to calculate the activation energy and the activation volume of the cement according to the basic kinetics theory of chemical reaction (Laidler, 1987):

$$\left(\frac{\partial \ln k}{\partial (1/T)}\right)_P = \frac{E_a}{R} \tag{10}$$

$$\left(\frac{\partial \ln k}{\partial (P)}\right)_T = -\frac{\Delta V^*}{RT} \tag{11}$$

Fig. 8 shows examples of fitted results of ultrasonic CS development (Eq. (7)) as well as transit time development (Eq. (9)), which indicate that the fitted curves are in excellent agreement with the original data curves. The complete list of fitted parameters (for both ultrasonic CS and transit time) as well as E_a estimated by linear regression analysis (Fig. 9) are shown in Table 4. The R-square values of the fitting to sonic strength test as well as transit time test results were almost equal to 1, indicating excellent agreements between model and original data. The ultimate sonic strength (S_u) showed relatively significant variations for tests at low temperature and high pressure (30 °C/50 MPa, 30 °C/100 MPa) as well as for tests at high temperature and low pressure (90 °C/5 MPa); fortunately, these conditions should be rarely encountered in the real field applications, considering that temperature and pressure typically increase simultaneously with well depth. When these special conditions were excluded, the S_u at various testing conditions exhibited smaller variations with an average value of 37.4 MPa and a standard deviation of 4.7 MPa. The initial transit time (t_S^I) of the cement slurries showed little dependence on curing temperature but strong dependence on curing pressure, with average values of 16.7 ± 0.23, 15.8 ± 0.19, and 14.9 ± 0.13 μs/in (i.e. 657.5 ± 9, 622 ± 7.5, and 586.6 ± 5.1 μs/m), for curing pressures of 5, 50, and 100 MPa, respectively. However, the final transit time at infinite time after cement setting (i.e. $t_S^I + t_S^u$) showed much weaker dependence on curing pressure with average values of 7.56, 7.40, and 7.33 μs/in (i.e. 297.6, 291.3, and 288.6 μs/m), for curing pressures of 5, 50, and 100 MPa, respectively. The final transit time at all curing temperatures and pressures has an overall result of 7.43 ± 0.24 μs/in (292.5 ± 9.4 μs/m). The different pressure dependence of transit time before and after cement setting is primarily due to the fact that cement slurry is much more compressible than set cement. The rate constants obtained from sonic strength (k) and transit time data (k_S^t) increased steadily with increasing temperature which seemed to be contrary to the qualitative observation in Fig. 7. This is primarily because the final sonic strength evolution profile is simultaneously affected by the rate constants and the ultimate sonic strength (S_u). The rate constants were used to calculate the apparent activation energy (E_a). As can be seen from Fig. 9, E_a derived by linear regression method based on different dataset varied within a relatively small range from 23.6 to 27.7 kJ/mol for different curing pressures, and the overall average result was 25.87 ± 1.38 kJ/mol.

Figs. 10 and 11 present the effect of curing pressure on the evolution of ultrasonic CS as well as P-wave velocity of the setting cement by UCA test. Apparently, while increasing curing temperature might lead to reductions in ultrasonic properties of the set

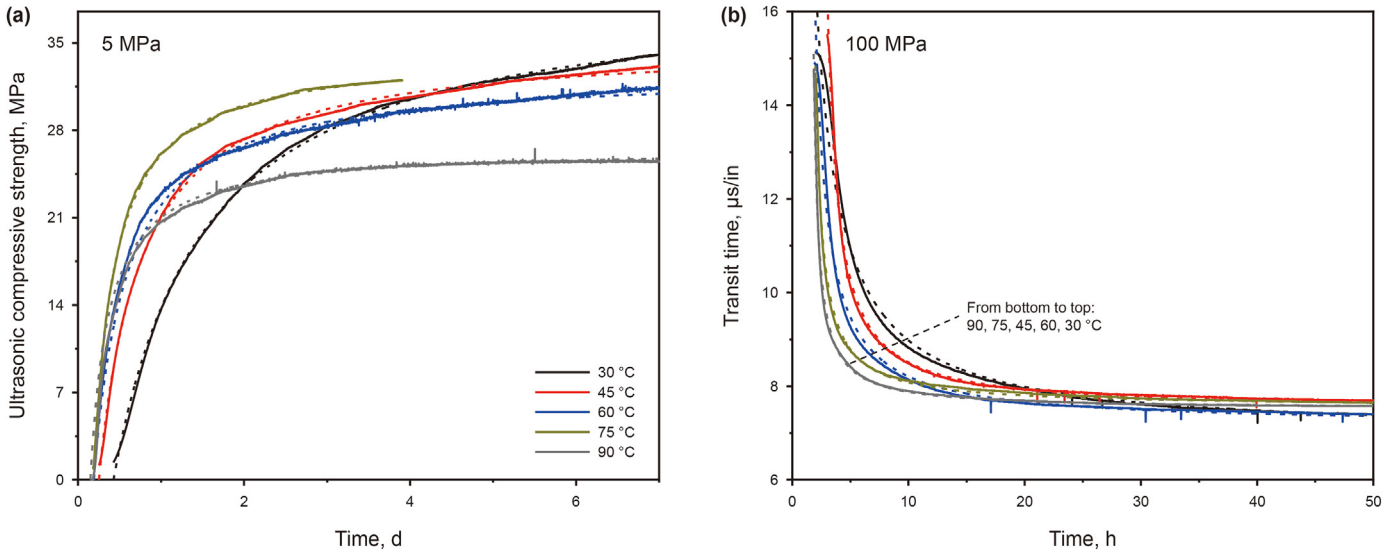

Fig. 8. Representative fitting results of experimental data (solid line: experimental test curves, dotted line: fitted curves by Eqs. (7) and (9), respectively).

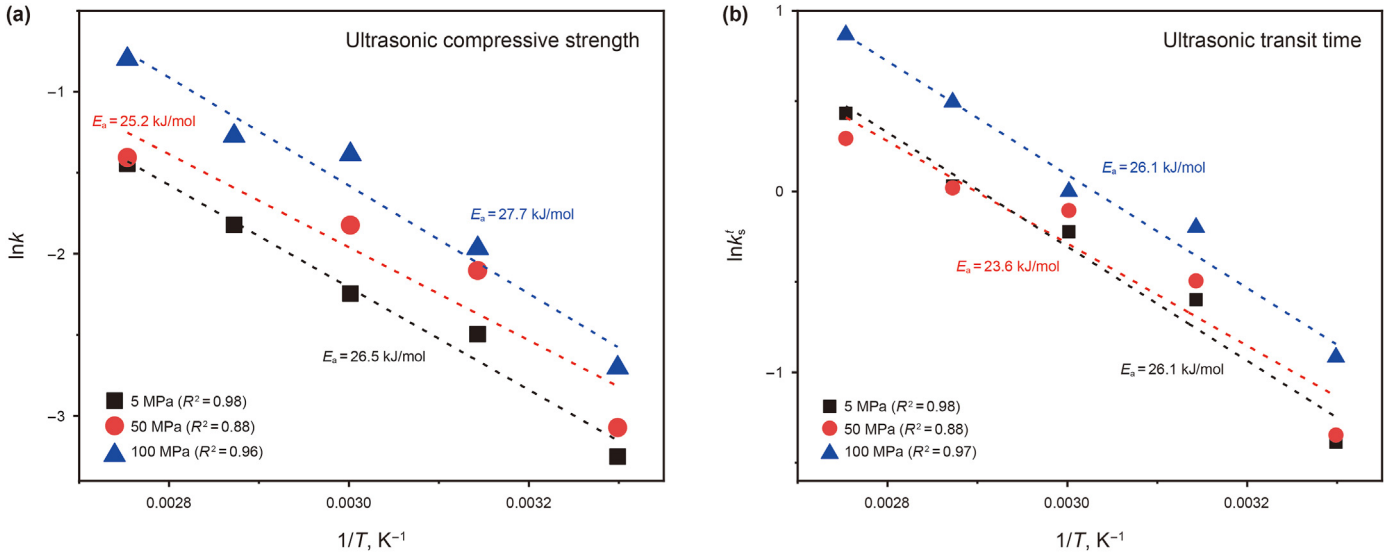

Fig. 9. Derivation of activation energy (E_a) of Class G cement using rate constants (k and k_S^t) in Table 4 and Eq. (10).

cement in the long term (Fig. 7), increasing curing pressure generally led to increases of these parameters. The starting point of strength development and P-wave velocity change (which is an indicator of setting time) appeared much earlier at higher curing pressures and the time it took for ultrasonic property to reach a stable stage generally decreased with increasing pressure, due to acceleration effect similar to temperature. Increasing curing pressure can significantly accelerate the ultrasonic property development and increase the ultimate values at all temperatures except for 75 °C. With curing pressure increasing from 5 to 100 MPa, the ultimate ultrasonic CS of cement cured at 30, 45, 60, and 90 °C was increased by 26.7%, 19.5%, 13.7%, and 32.1%, respectively. The effect of curing pressure on the ultrasonic CS evolution of the cement at 75 °C was much weaker than at other temperatures, and the final ultrasonic CS at curing time beyond 70 h were almost equal for all pressures. Similarly, the P-wave velocity of cement samples under different pressures were almost equal during 50–100 h at 75 °C.

The rate constants shown in Table 4 can also be used to derive ΔV^* at different temperatures and the results obtained by linear regression analysis are shown in Fig. 12. ΔV^* varied somewhat randomly with temperature and no clear trend of variation can be observed. The values obtained from ultrasonic CS data varied within a range from −14.4 to −23.8 cm^3/mol (Fig. 12a), which has an average of −18.2 cm^3/mol and a standard deviation of 3.8 cm^3/mol. However, the magnitudes of ΔV^* derived based on transit time data were apparently lower (Fig. 12b), especially at 60 °C (−6.4 cm^3/mol). Except for 60 °C, the values obtained from transit time data varied within a relatively small range from −11.1 to −14.2 cm^3/mol, with an overall results of −13.1 ± 1.56 cm^3/mol. These results showed that curing temperature seems to have little to no influence on ΔV^* obtained by the transit time data as well as ultrasonic CS data. The relatively large variations can be attributed to experimental errors as well as limitations of the model, especially considering that the curing pressure has a much smaller effect on property evolution than curing temperature.

Table 4
The best-fit parameters based on Eqs. (7) and (9) for different conditions.

Conditions		Based on ultrasonic compressive strength				Based on transit time				
P, MPa	T, °C	t_0, h	S_u, MPa	k, 1/h	E_a[a], kJ/mol	t_0, h	t_S^l[b], μs/in	t_S^u, μs/in	k_S^t, 1/h	E_a[a], kJ/mol
5	30	10.2	39.6	0.039	26.5	9.00	16.84	−9.560	0.25	26.1
	45	6.07	35.2	0.08		5.87	16.61	−9.106	0.55	
	60	4.59	32.7	0.11		4.67	16.55	−8.953	0.80	
	75	4.39	34.2	0.16		4.06	16.52	−9.023	1.03	
	90	3.59	26.6	0.24		3.44	17.07	−9.155	1.54	
50	30	4.96	45.7	0.05	25.2	3.86	15.9	−8.910	0.26	23.6
	45	3.68	34.1	0.12		3.33	16.13	−8.635	0.61	
	60	3.05	34.7	0.16		2.94	15.72	−8.256	0.90	
	75	2.97	34.1	0.20		2.70	15.66	−8.180	1.02	
	90	3.26	32.8	0.25		3.14	15.79	−8.243	1.34	
100	30	2.47	47.5	0.067	27.7	2.38	15.14	−8.158	0.40	26.1
	45	2.16	42.1	0.14		2.13	14.91	−7.738	0.82	
	60	1.70	36.0	0.25		2.98	14.82	−7.401	1.00	
	75	1.85	33.2	0.28		1.99	14.82	−7.253	1.64	
	90	1.87	33.8	0.45		1.85	14.85	−7.330	2.38	

Note.
[a] E_a is the value of apparent activation energy derived in the temperature range of 30–90 °C by linear regression analysis (See Fig. 9).
[b] Initial value of transit time obtained from original experimental data after temperature and pressure has stabilized.

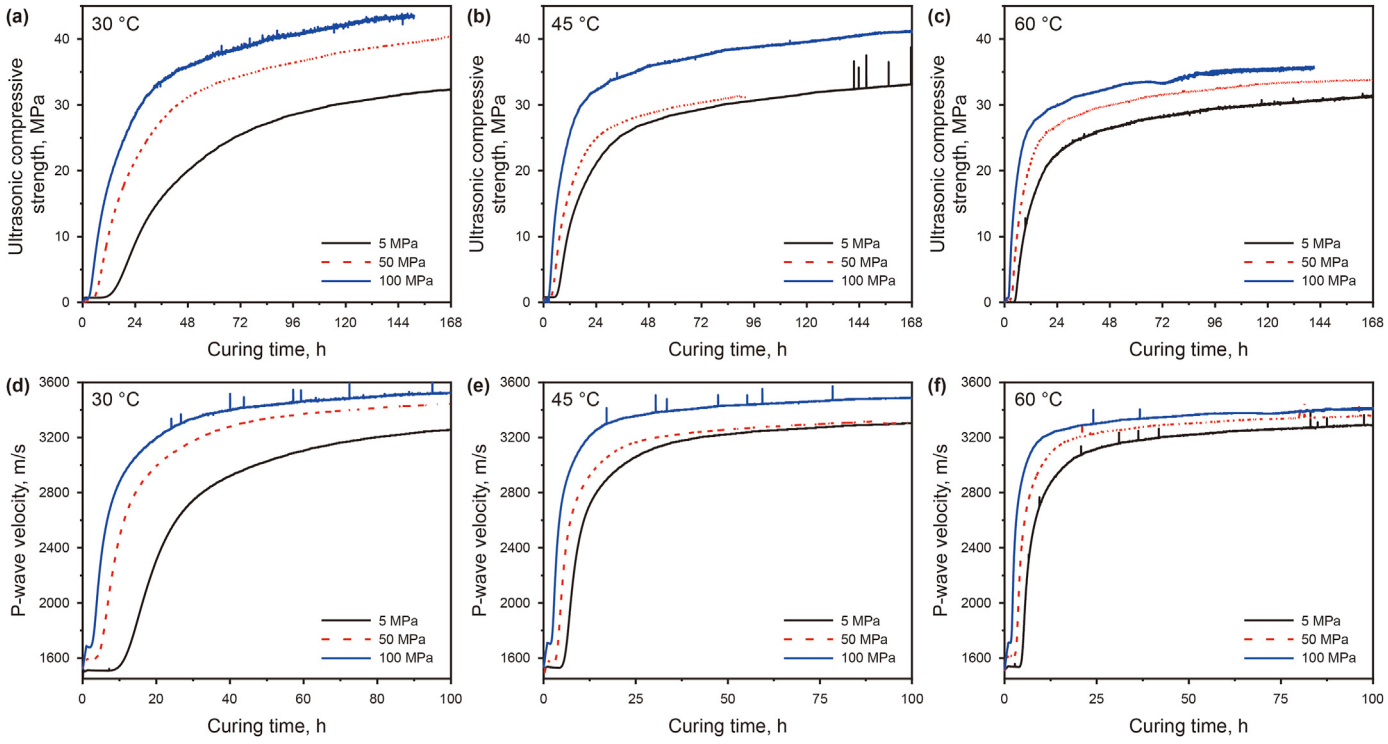

Fig. 10. Effects of curing pressure on the ultrasonic property evolution of cement slurry by UCA (35, 45, and 60 °C).

4.4. Dependences of E_a and ΔV^* on test methods

Since E_a and ΔV^* are two of the most important parameters of the scale factor model, it is highly critical to evaluate their dependences on the different test methods of this study. The E_a derived by IC test was compared with those obtained by thickening time test and UCA test at 0–5 MPa in Fig. 13. The test temperature range for various experimental methods was from 30 to 90 °C. The R-square values of the linear fittings were all higher than 0.97, indicating excellent agreements between model and experimental data. The values of E_a obtained from ultrasonic CS, ultrasonic transit time (TT), and thickening time test data were all in excellent agreements, with an average of 25.7 kJ/mol, while E_a derived from IC test data was around 32% higher. Therefore, it can be concluded that the curing temperature has a stronger effect on cement hydration rate than physical property development rate.

By comparing thickening time test results (Table 2) and UCA test results (Fig. 9), it can be seen that E_a obtained by thickening time tests was about 35% lower than that obtained by UCA tests at 50 MPa curing pressure. This may be due to experimental uncertainties, considering that the results obtained by thickening time was highly variable. At 30 °C, ΔV^* obtained by thickening time tests (Table 3) was 270% higher than that derived by UCA tests (Fig. 10), while at 75 °C, ΔV^* obtained by thickening time tests was

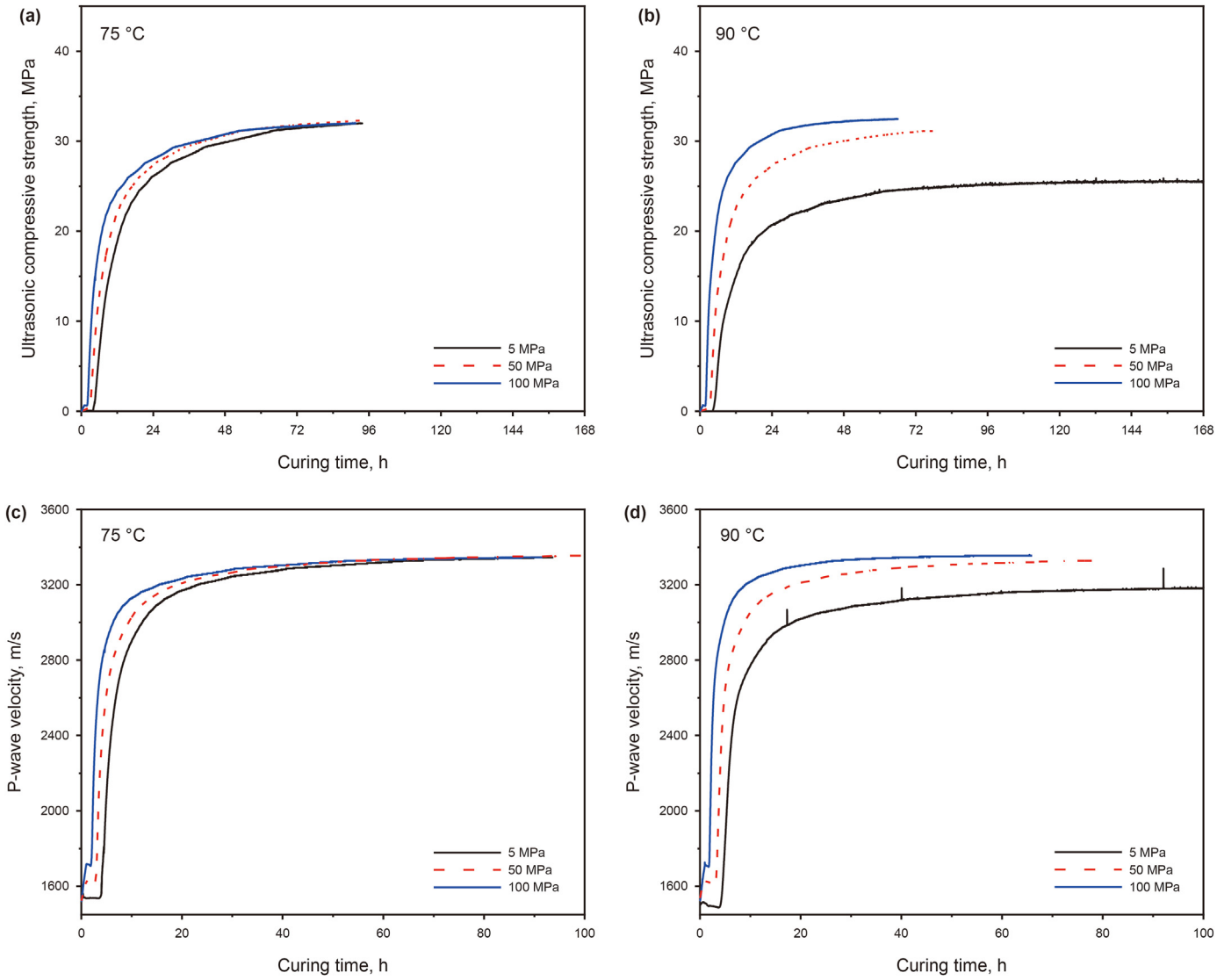

Fig. 11. Effects of curing pressure on the ultrasonic property evolution of cement slurry by UCA (75 and 90 °C).

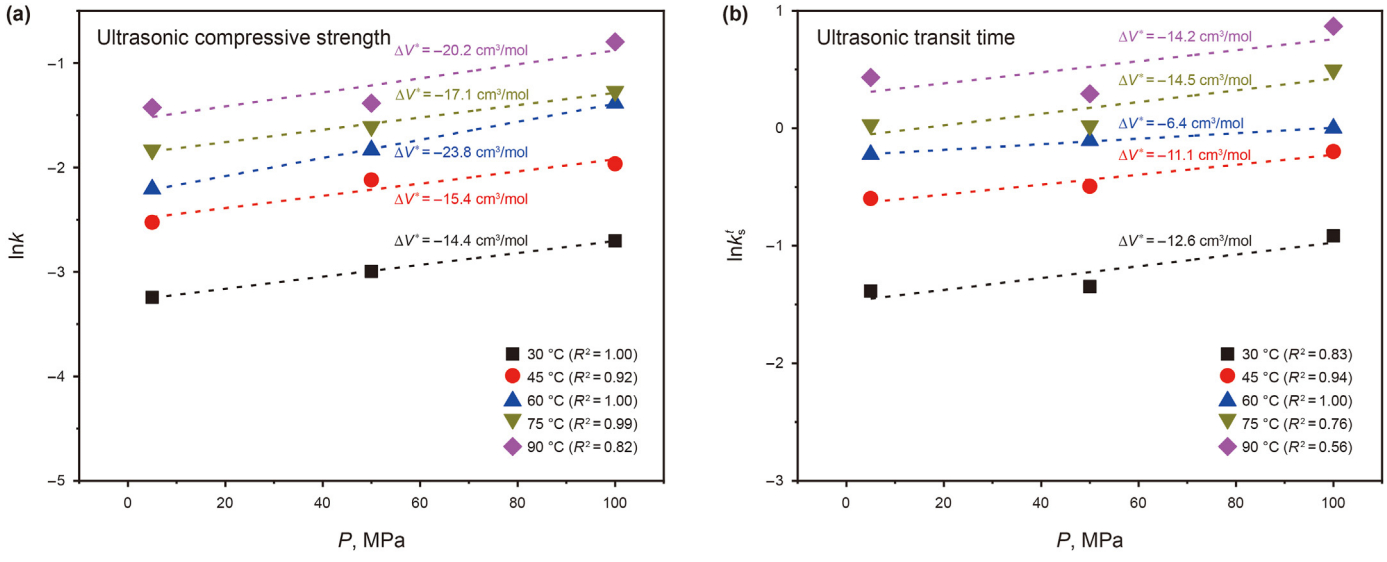

Fig. 12. Derivation of ΔV^* of Class G cement using rate constants (k and k_S^t) in Table 4 and Eq. (11).

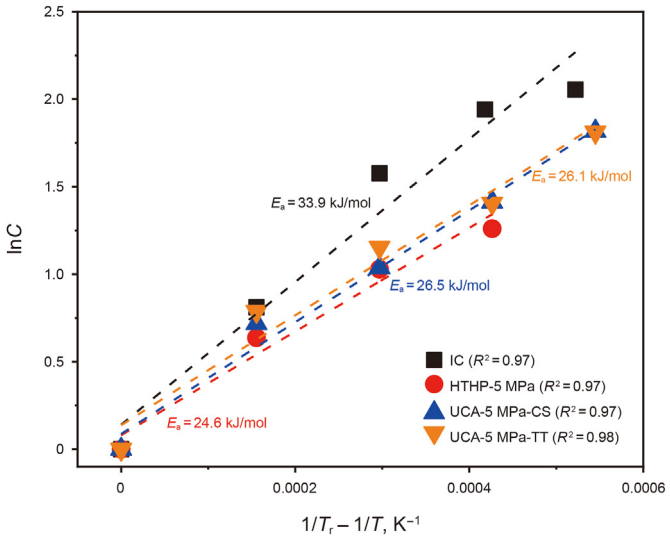

Fig. 13. Linear fits as used to obtain the E_a based on different methods.

70% higher than that derived by UCA tests. Thickening time test measures the early age property evolution of cement slurries before setting, while UCA test is primarily focused on the property evolution after setting. The test results suggest that curing pressure has much stronger influences on cement property evolution rate before setting, compared to after setting. It should be noted that averaged results from UCA sonic strength and UCA transit time were used for the comparison here, since their differences were relatively small (7%–15%).

4.5. Setting time estimate comparisons

Setting time is one of the most important properties for cement-basted materials during both oil well cementing operations and building constructions. The setting time of cement can be estimated by various test methods, such as penetration resistance method (ASTM C403, 2017), ultrasonic wave method (Lee et al., 2004), Vicat Needle method (ASTM C191-21, 2021), etc. As mentioned previously, thickening time represents the time at which a cement slurry loses its pumpability, which can be approximated as the setting time (ST_{Bc}). An UCA test measures the continuous development of a cement slurry's sonic strength, and the start point of strength gain can be approximated as the setting time of cement as well (ST_{UCA}). In the oil well cementing industry, ST_{UCA} is sometimes simply determined as the point of time when the ultrasonic strength reaches a small value (such as 0.4 MPa). In this study, ST_{UCA} was determined by the intersection point of two linear line fitting to the ultrasonic CS test data obtained during early hydration period: the first line had an almost zero slope, the second line had a slope that represents the initial strength development rate. During this period of slope change, more and more cement grains that were initially suspended in water became interconnected as newly formed hydration products filled the space originally occupied by water. More detailed information about how to determine this point can be found in Lee et al. (2004). The end of the induction period during cement hydration signifies the start point of accelerated cement hydration, which is another approximation for setting time (ST_{HOH}). Table 5 compares the setting time estimated by these different test methods, which were apparently in reasonable agreement with each other. All test results showed that setting time decreased with increasing temperature and pressure. However, the temperature effect on setting time was very small in the range between 60 and 90 °C. Most of the time, the set time determined by UCA was slightly longer than that determined by thickening time tests.

Table 5
The initial setting times obtained by different test methods under different curing conditions.

Pressure, MPa	Methods	Initial setting time at different temperatures, h				
		30 °C	45 °C	60 °C	75 °C	90 °C
5	ST_{Bc}	8.38	4.66	3.13	2.51	2.64
	ST_{UCA}	6.23	4.58	4.00	3.53	3.17
	ST_{HOH}	7.25[a]	4.79[a]	4.09[a]	4.10[a]	3.40[a]
50	ST_{Bc}	3.94	2.65	2.23	1.87	1.94
	ST_{UCA}	3.44	2.93	2.45	2.68	2.30
100	ST_{Bc}	1.88	–	–	1.38	–
	ST_{UCA}	2.03	1.90	1.65	1.84	1.77

Note:
[a] Obtained by an isothermal calorimeter at atmospheric pressure.

4.6. Discussion

The hydration reactions of cement result in continuous variations of physical and mechanical properties (such as hydration heat, viscosity and sonic transit time) of the cement-based materials. While hydration heat has an approximately linear relationship with degree of hydration and is a commonly used metrics to measure cement hydration kinetics, viscosity, and sonic properties of the cement clearly have intrinsic dependencies on temperature and pressure and their correlations with degree of hydration are not unique. In other words, cement materials with the same degree of hydration could exhibit different viscosities and sonic properties, due to differences in microstructure and morphology of hydration products obtained at different curing temperatures and pressures. Thus, the critical parameters in the scale factor model, i.e. E_a and ΔV^*, do not carry their original physical meanings and instead are simply fitting parameters, when cement properties not directly associated with degree of hydration are considered. This is the reason why the two parameters show strong dependences on the type of material property being modeled. Nevertheless, it can be seen from the results of this study that the scale factor model developed from chemical kinetics theories works quite well in reproducing the effects of curing temperature and pressure on the various property evolution of Class G cement. Therefore, from an engineering perspective, the two fitted parameters (E_a and ΔV^*) can still be used to gauge the sensitivity of a particular property development rate on curing temperature and pressure, respectively.

5. Conclusions

The influences of temperature and pressure on the hydration, viscosity and acoustic property evolution of Class G oil well cement were investigated experimentally and simulated based on a scale factor model. The following conclusions can be drawn.

(1) Both curing temperature and curing pressure can accelerate cement hydration, which leads to increases in hydration heat release rate as well as viscosity and sonic property evolution rate in the early stage of cement hydration. However, the overall acceleration effects varied significantly with test methods and actual curing conditions.
(2) The apparent activation energy (E_a) of the cement, which represents the temperature sensitivity of property evolution rate for a constant pressure process, showed significant

reductions with increasing curing temperature according to hydration heat and viscosity evolution test results. However, E_a obtained from sonic property evolution after setting showed little dependence on curing temperature and pressure, with an average of 25.87 kJ/mol.

(3) The apparent activation volume (ΔV^*) of the cement, which represents the pressure sensitivity of property evolution rate for a constant temperature process, mostly showed little dependence on curing temperature except for some outliers. ΔV^* obtained from viscosity evolution measurement at various temperatures (except for 30 °C) has an average of −29.8 cm^3/mol, while that obtained from sonic strength evolution has an average of −18.2 cm^3/mol, suggesting curing pressure has a much stronger influence on cement slurry properties before setting than after setting of cement.

(4) The ultimate physical and mechanical properties (P-wave velocity and ultrasonic compressive strength) of set cement estimated by ultrasonic testing decreased with increasing curing temperature and increased with increasing curing pressure.

(5) The setting time of cement approximated by the end of induction period of heat of hydration test, thickening time of a cement slurry and the starting time of sonic strength gain were in reasonable agreement with each other at different curing temperatures and pressures.

Declaration of competing interest

The authors declare that they have no known competing financial interests or personal relationships that could have appeared to influence the work reported in this paper.

Acknowledgements

Financial support comes from China National Natural Science Foundation (No. 51974352) as well as from China University of Petroleum (East China) (No. 2018000025 and No. 2019000011).

References

API RP 10B-2, 2013. Recommended Practice for Testing Well Cements. https://global.ihs.com/doc_detail.cfm?&rid=GS&document_name=API%20RP%2010B%2D2&item_s_key=00464011&item_key_date=800831.

ASTM C1608-17, 2017. Standard Test Method for Chemical Shrinkage of Hydraulic Cement Paste. ASTM International, West Conshohocken, p. 5. https://www.astm.org/standards/c1608.

ASTM C403, 2017. Standard Test Method for Time of Setting of Concrete Mixtures by Penetration Resistance. Annual Books of ASTM Standards, ASTM, Philadelphia, USA, p. 7. https://www.astm.org/c0403_c0403m-08.html.

ASTM C1074-19, 2019. Standard Practice for Estimating Concrete Strength by the Maturity Method. ASTM International, West Conshohocken, p. 10. https://www.astm.org/c1074-19.html.

ASTM C191-21, 2021. Standard Test Methods for Time of Setting of Hydraulic Cement by Vicat Needle. ASTM International, p. 8. https://www.astm.org/c0191-21.html.

Bergold, S.T., Goetz-Neunhoeffer, F., Neubauer, J., 2013. Quantitative analysis of C-S-H in hydrating alite pastes by in-situ XRD. Cement Concr. Res. 53, 119–126. https://doi.org/10.1016/j.cemconres.2013.06.001.

Chidiac, S.E., Moutassem, F., Mahmoodzadeh, F., 2013. Compressive strength model for concrete. Mag. Concr. Res. 65 (9), 557–572. https://doi.org/10.1680/macr.12.00167.

Chidiac, S.E., Shafikhani, M., 2019. Cement degree of hydration in mortar and concrete. J. Therm. Anal. Calorim. 138 (3), 2305–2313. https://doi.org/10.1007/s10973-019-08800-w.

Delatte, N.J., Williamson, M.S., Fowler, D.W., 2000. Bond strength development with maturity of high-early-strength bonded concrete overlays. ACI Struct. J. 97 (2), 201–207. https://www.concrete.org/publications/internationalconcreteabstractsportal/m/details/id/824.

Du, J., Bu, Y., Cao, X., et al., 2018. Utilization of alkali-activated slag based composite in deepwater oil well cementing. Construct. Build. Mater. 186, 114–122. https://doi.org/10.1016/j.conbuildmat.2018.07.068.

Escalante-Garcia, J.I., 2003. Nonevaporable water from neat OPC and replacement materials in composite cements hydrated at different temperatures. Cement Concr. Res. 33 (11), 1883–1888. https://doi.org/10.1016/S0008-8846(03)00208-4.

Gallucci, E., Zhang, X., Scrivener, K.L., 2013. Effect of temperature on the microstructure of calcium silicate hydrate (C-S-H). Cement Concr. Res. 53, 185–195. https://doi.org/10.1016/j.cemconres.2013.06.008.

Gómez-Zamorano, L.Y., Escalante-García, J.I., 2010. Effect of curing temperature on the nonevaporable water in portland cement blended with geothermal silica waste. Cem. Concr. Compos. 32 (8), 603–610. https://doi.org/10.1016/j.cemconcomp.2010.07.004.

Hesse, C., Goetz-Neunhoeffer, F., Neubauer, J., 2011. A new approach in quantitative in-situ XRD of cement pastes: correlation of heat flow curves with early hydration reactions. Cement Concr. Res. 41 (1), 123–128. https://doi.org/10.1016/j.cemconres.2010.09.014.

Jansen, D., Goetz-Neunhoeffer, F., Lothenbach, B., et al., 2012. The early hydration of Ordinary Portland Cement (OPC): an approach comparing measured heat flow with calculated heat flow from QXRD. Cement Concr. Res. 42, 134–138. https://doi.org/10.1016/j.cemconres.2011.09.001.

Jensen, O.M., Hansen, P.F., 1999. Influence of temperature on autogenous deformation and relative humidity change in hardening cement paste. Cement Concr. Res. 29 (4), 567–575. https://doi.org/10.1016/S0008-8846(99)00021-6.

Jupe, A.C., Wilkinson, A.P., Funkhouser, G.P., 2012a. The effect of pressure on tricalcium silicate hydration at different temperatures and in the presence of retarding additives. Cement Concr. Res. 42 (8), 1083–1087. https://doi.org/10.1016/j.cemconres.2012.04.008.

Jupe, A.C., Wilkinson, A.P., Funkhouser, G.P., 2012b. Simultaneous study of mechanical property development and early hydration chemistry in Portland cement slurries using X-ray diffraction and ultrasound reflection. Cement Concr. Res. 42 (8), 1166–1173. https://doi.org/10.1016/j.cemconres.2012.05.013.

Kada-Benameur, H., Wirquin, E., Duthoit, B., 2000. Determination of apparent activation energy of concrete by isothermal calorimetry. Cement Concr. Res. 30 (2), 301–305. https://doi.org/10.1016/S0008-8846(99)00250-1.

Kjellsen, K.O., Detwiler, R.J., Gjørv, O.E., 1991. Development of microstructures in plain cement pastes hydrated at different temperatures. Cement Concr. Res. 21 (1), 179–189. https://doi.org/10.1016/0008-8846(91)90044-I.

Kjellsen, K.O., Detwiler, R.J., 1992. Reaction kinetics of Portland cement mortars hydrated at different temperatures. Cement Concr. Res. 22 (1), 112–120. https://doi.org/10.1016/0008-8846(92)90141-H.

Kupwade-Patil, K., Boul, P.J., Rasner, D.K., et al., 2019. Retarder effect on hydrating oil well cements investigated using in situ neutron/X-ray pair distribution function analysis. Cement Concr. Res. 126, 105920. https://doi.org/10.1016/j.cemconres.2019.105920.

Krauß, M., Hariri, K., 2001. Determination of initial degree of hydration for improvement of early-age properties of concrete using ultrasonic wave propagation. Cem. Concr. Compos. 28 (4), 299–306. https://doi.org/10.1016/j.cemconcomp.2006.02.007.

Laidler, K.J., 1987. Chemical Kinetics, third ed. Harper & Row Publishers.

Lee, H.K., Lee, K.M., Kim, Y.H., et al., 2004. Ultrasonic in-situ monitoring of setting process of high-performance concrete. Cement Concr. Res. 34 (4), 631–640. https://doi.org/10.1016/j.cemconres.2003.10.012.

Li, X., Yang, H., Li, M., 2014. Assessment of hydration degree of cement in the fly ash-cement pastes based on the calcium hydroxide content. Adv. Mater. Res. 875–877, 177–182. https://doi.org/10.4028/www.scientific.net/AMR.875-877.177.

Liao, W., Sun, X., Kumar, A., et al., 2019. Hydration of binary Portland cement blends containing silica fume: a decoupling method to estimate degrees of hydration and pozzolanic reaction. Front. Mater. 78 (6), 1–13. https://doi.org/10.3389/fmats.2019.00078.

Lura, P., Winnefeld, F., Klemm, S., 2010. Simultaneous measurements of heat of hydration and chemical shrinkage on hardening cement pastes. J. Therm. Anal. Calorim. 101 (3), 925–932. https://doi.org/10.1007/s10973-009-0586-2.

Ma, S., Kawashima, S., 2019. A rheological approach to study the early-age hydration of oil well cement: effect of temperature, pressure and nanoclay. Construct. Build. Mater. 215, 119–127. https://doi.org/10.1016/j.conbuildmat.2019.04.177.

Meng, M., Frash, L., Carey, J.W., et al., 2021. Predicting cement-sheath integrity with consideration of initial state of stress and thermoporoelastic effects. SPE J. 26, 3505–3528. https://doi.org/10.2118/205344-PA.

Pang, X., 2014. A generalized scale factor model for Portland cement hydration. In: The 4th RILEM International Symposium on Concrete Modelling.

Pang, X., Meyer, C., 2012. Cement chemical shrinkage as measure of hydration kinetics and its relationship with nonevaporable water. ACI Mater. J. 109 (3), 341–352. https://www.concrete.org/publications/internationalconcreteabstractsportal.aspx?m=details&id=51683825.

Pang, X., Bentz, D.P., Meyer, C., et al., 2013a. A comparison study of Portland cement hydration kinetics as measured by chemical shrinkage and isothermal calorimetry. Cem. Concr. Compos. 39, 23–32. https://doi.org/10.1016/j.cemconcomp.2013.03.007.

Pang, X., Cuello, J.W., Iverson, B.J., 2013b. Hydration kinetics modeling of the effect of curing temperature and pressure on the heat evolution of oil well cement. Cement Concr. Res. 54, 69–76. https://doi.org/10.1016/j.cemconres.2013.08.014.

Pang, X., Meyer, C., Darbe, R., et al., 2013c. Modeling the effect of curing temperature and pressure on cement hydration kinetics. ACI Mater. J. 110 (2), 137–148. https://www.concrete.org/publications/internationalconcreteabstractsportal.aspx?m=details&id=51685528.

Pang, X., Otieno, P., Funkhouser, G.P., 2014. Modeling the effect of curing pressure on

the viscosity evolution of oilwell cement. In: The 2014 AADE Fluid Technical Conference & Exhibition. https://www.aade.org/application/files/1315/7260/3862/AADE-14-FTCE-06.pdf.

Pang, X., Jimenez, W.C., Singh, J.P., 2020. Measuring and modeling cement hydration kinetics at variable temperature conditions. Construct. Build. Mater. 262, 120788. https://doi.org/10.1016/j.conbuildmat.2020.120788.

Pang, X., Sun, L., Sun, F., et al., 2021. Cement hydration kinetics study in the temperature range from 15 °C to 95 °C. Cement Concr. Res. 148, 106552. https://doi.org/10.1016/j.cemconres.2021.106552.

Pang, X., Sun, L., Chen, M., et al., 2022. Influence of curing temperature on the hydration and strength development of Class G Portland cement. Cement Concr. Res. 156, 106776. https://doi.org/10.1016/j.cemconres.2022.106776.

Peethamparan, S., Weissinger, E., Vocaturo, J., et al., 2010. Monitoring chemical shrinkage using pressure sensors. Adv. Mater. Sci. Concr. 270 (7), 77–88. https://www.concrete.org/publications/internationalconcreteabstractsportal/m/details/id/51663740.

Pichler, C., Schmid, M., Traxl, R., et al., 2017. Influence of curing temperature dependent microstructure on early-age concrete strength development. Cement Concr. Res. 102, 48–59. https://doi.org/10.1016/j.cemconres.2017.08.022.

Pinto, R., Hover, K.C., 1999. Application of maturity approach to setting times. ACI Mater. J. 96 (6), 686–690. https://www.concrete.org/publications/internationalconcreteabstractsportal/m/details/id/795.

Reinhardt, H.W., Grosse, C.U., 2004. Continuous monitoring of setting and hardening of mortar and concrete. Construct. Build. Mater. 18 (3), 145–154. https://doi.org/10.1016/j.conbuildmat.2003.10.002.

Robeyst, N., Gruyaert, E., Grosse, C.U., et al., 2008. Monitoring the setting of concrete containing blast-furnace slag by measuring the ultrasonic p-wave velocity. Cement Concr. Res. 38 (10), 1169–1176. https://doi.org/10.1016/j.cemconres.2008.04.006.

Scherer, G.W., Funkhouser, G.P., Peethamparan, S., 2010. Effect of pressure on early hydration of class H and white cement. Cement Concr. Res. 40 (6), 845–850. https://doi.org/10.1016/j.cemconres.2010.01.013.

Sun, L., Pang, X., Bu, Y., et al., 2021a. Experimental study of the effect of curing temperature and pressure on the property evolution of oilwell cement. In: The ARMA 55th US Rock Mechanics/Geomechanics Symposium. In: https://onepetro.org/ARMAUSRMS/proceedings-abstract/ARMA21/All-ARMA21/ARMA-2021-1397/468031.

Sun, L., Pang, X., Guo, S., et al., 2021b. Simulations of hydration kinetics of portland cement by scale factor method. J. Chin. Ceram. Soc. 49 (5), 1–10 (in Chinese). https://kns.cnki.net/kcms/detail/detail.aspx?dbcode=CJFD&dbname=CJFDLAST2021&filename=GXYB202105014&uniplatform=NZKPT&v=QWHO_UCwxC0fD0GAQJF_lpsiYoXqGzT8mZIeAnN1ecXuuAZQZW9Oiqj3UbAlpPpH.

Sun, F., Pang, X., Kawashima, S., et al., 2022. Effect of tartaric acid on the hydration of oil well cement at elevated temperatures between 60 °C and 89 °C. Cement Concr. Res. 161, 106952. https://doi.org/10.1016/j.cemconres.2022.106952.

Taylor, H.F.W., 1997. Cement Chemistry, second ed. Thomas Telford Publishing, London. https://doi.org/10.1680/cc.25929.

Turcry, P., Loukili, A., Barcelo, L., et al., 2002. Can the maturity concept be used to separate the autogenous shrinkage and thermal deformation of a cement paste at early age? Cement Concr. Res. 32 (9), 1443–1450. https://doi.org/10.1016/S0008-8846(02)00800-1.

Voigt, T., Sun, Z., Shah, S.P., 2006. Comparison of ultrasonic wave reflection method and maturity method in evaluating early-age compressive strength of mortar. Cem. Concr. Compos. 28 (4), 307–316. https://doi.org/10.1016/j.cemconcomp.2006.02.003.

Zhang, J., Cusson, D., Monteiro, P., et al., 2008. New perspectives on maturity method and approach for high performance concrete applications. Cement Concr. Res. 38 (12), 1438–1446. https://doi.org/10.1016/j.cemconres.2008.08.001.

Zhang, W., Zhang, Y., Liu, L., et al., 2012. Investigation of the influence of curing temperature and silica fume content on setting and hardening process of the blended cement paste by an improved ultrasonic apparatus. Construct. Build. Mater. 33, 32–40. https://doi.org/10.1016/j.conbuildmat.2012.01.011.